

## Mechanism for electric dipole transitions from the broad $p$ -wave neutron resonance in $^{24}\text{Mg}$

T. Uchiyama, M. Igashira, and H. Kitazawa

*Research Laboratory for Nuclear Reactors, Tokyo Institute of Technology, 2-12-1 O-okayama, Meguro-ku, Tokyo 152, Japan*

(Received 20 July 1989)

Neutron capture gamma rays from the 84-keV  $p_{3/2}$ -wave resonance, 266-keV  $p_{1/2}$ -wave resonance, and 431-keV  $p_{3/2}$ -wave resonance in  $^{24}\text{Mg}$  that have large reduced neutron width have been measured with an anti-Compton NaI(Tl) detector, using a time-of-flight technique. Successful extraction of gamma-ray intensities for transitions to low-lying states in  $^{25}\text{Mg}$  was performed by an iterative unfolding method, in order to deduce partial radiative widths. Also, we have made an experimental contrivance separating the kernel of the 266-keV broad resonance from that of the 257-keV overlapping narrow resonance. Radiative widths were obtained for the  $E1$  transitions to the ground ( $\frac{5}{2}^+$ ), 585-keV ( $\frac{1}{2}^+$ ), 975-keV ( $\frac{3}{2}^+$ ), 1965-keV ( $\frac{5}{2}^+$ ), 2564-keV ( $\frac{1}{2}^+$ ), and 2801-keV ( $\frac{3}{2}^+$ ) states, and were compared with theoretical calculations based on the valence capture model that was developed by Lane and Mughabghab. Consequently, we found that in the  $p_{3/2}$ -wave resonance capture the observed and calculated widths for the transitions to the  $\frac{1}{2}^+$  states are in excellent agreement; however, the experimental widths for the transitions to the  $\frac{5}{2}^+$  states are 20–50% of the theoretical ones. These noteworthy features in the retardation of  $E1$  transition are explained in terms of the renormalized effective charge, which depends on the orbital angular momentum for the single-particle component of final bound states, as a result of the coupling of the single-particle transition with the isovector field generated by the giant dipole resonance. Moreover, the nonadiabatic coupled-channel calculation using a particle-rotator coupling model was carried out for partial radiative widths of the 266-keV  $p_{1/2}$ -wave resonance. The calculations reproduced the observed values satisfactorily.

### I. INTRODUCTION

Neutron transmission experiments have revealed many nuclear resonance levels in the vicinity of the neutron binding energy, and consequently revealed the statistical behaviors of the width and distance of these levels, characterized by the Porter-Thomas and Wigner distributions, respectively. Besides, elaborate investigations on the nuclear structure of resonance states have been performed through the well-known electromagnetic interaction with nuclei. The reason is that, while the single-particle component of a resonance state is projected on the emitted neutron channel, the primary electromagnetic transitions provide a detailed knowledge of the particle configuration of the resonance state. As a result, nonstatistical properties of neutron resonance-capture reactions, such as correlations between reduced neutron widths and total radiative widths, and those between reduced partial radiative widths and spectroscopic factors of low-lying states, were found over a wide mass region.

In neutron resonance-capture reactions, our particular interest was aroused in gamma-ray transitions from  $s$ - and  $p$ -wave resonances with large reduced neutron width. From the uncertainty principle, broad resonances are expected to have a simple configuration, 1p-0h or 2p-1h. In fact, some strong single-particle  $E1$  transitions have been observed from broad resonances to low-lying states with a large spectroscopic factor.<sup>1,2</sup> These transitions are theoretically understood as being caused by the decou-

pling of single-particle states from the giant dipole resonance (GDR),<sup>3</sup> and are in striking contrast with the extreme retardation of the  $E1$  transition between bound states. Here, the decoupling is generated by the boundary-condition mixing of  $s$ - and  $p$ -wave neutron states<sup>4</sup> and/or by the diagonalization of particle-hole interaction matrix elements using a realistic nuclear force.<sup>5</sup>

Lane and Lynn<sup>6</sup> have proposed a valence-capture theory in order to explain the strong  $E1$  transition following neutron resonance capture in nuclei. In the framework of the optical-potential model, this theory has been developed by Lane and Mughabghab<sup>7</sup> into a useful formalization, which is nearly independent of a choice of potential parameters. In these theories, only the entrance-channel component of the resonance state wave function was assumed to be dominant in  $E1$  transition.

From a weak-coupling model, however, there are also some indications<sup>8</sup> that collective states of a target nucleus are strongly reflected on the nuclear structure of broad resonances near the neutron emission threshold. Halder-son *et al.*<sup>9</sup> stressed the importance of core excitation in the broad  $s$ - and  $p$ -wave neutron resonances in calculating the neutron strength function of  $^{28}\text{Si}$  with a particle-vibration coupling model. Similarly, Kitazawa *et al.*<sup>10</sup> found substantial agreement between observed and calculated partial radiative widths for  $E1$  transitions from the 565-keV  $p_{3/2}$ -wave resonance in  $^{28}\text{Si}$ , taking account of the  $2^+$  and  $3^-$  one-phonon excitations of the  $^{28}\text{Si}$  core nucleus in the resonance state.

On the other hand, available experimental data on the total radiative width of broad resonances have been found to frequently include some systematic error.<sup>11</sup> This problem is in particular serious for the data measured with neutron-sensitive total energy detectors in time-of-flight experiments using an electron linear accelerator. In these experiments it is intrinsically difficult to resolve capture gamma-ray events and the background due to the neutrons scattered in the capture sample.

From this viewpoint, the present study was directed to  $E1$  transitions from broad  $p$ -wave resonances in  $^{24}\text{Mg}$ . So far, three broad  $p$ -wave resonances in  $^{24}\text{Mg}$  have been observed in neutron transmission experiments below the 1-MeV neutron energy: 84-keV  $p_{3/2}$ -wave resonance ( $\Gamma_n = 7.7 \pm 0.5$  keV), 266-keV  $p_{1/2}$ -wave resonance ( $\Gamma_n = 78 \pm 1$  keV), and 431-keV  $p_{3/2}$ -wave resonance ( $\Gamma_n = 31 \pm 1$  keV).<sup>12-16</sup> Weigmann *et al.*<sup>14</sup> have measured total radiative widths of neutron resonance states in  $^{24}\text{Mg}$  at the Oak Ridge electron linear accelerator time-of-flight facilities. The data for five  $p$ -wave resonances below the 1-MeV neutron energy produced a fairly large correlation coefficient [ $\rho(\Gamma_\gamma, \gamma_n^2) = 0.57$ ] between reduced neutron widths and total radiative widths. Furthermore, Bergqvist *et al.*<sup>17</sup> have measured the gamma-ray spectrum from the 84-keV neutron resonance capture in  $^{24}\text{Mg}$ , and extracted partial radiative widths of the resonance. As pointed out by Lane<sup>18</sup> and Mughabghab,<sup>19</sup> these results have disclosed a positive correlation [ $\rho(\Gamma_{\gamma_f} / E_\gamma^3, \theta_f^2) = 0.64$ ] between reduced partial radiative widths and spectroscopic factors of low-lying states.

The  $^{24}\text{Mg}$  nucleus is located in the mass region where the  $p$ -wave neutron strength function reaches a peak. Also, the reduced neutron widths of three broad  $p$ -wave resonances mentioned above account for a considerable fraction of the Wigner limit: 8.2% for the 84-keV resonance, 16.6% for the 266-keV resonance, and 3.6% for the 431-keV resonance. Therefore, it is expected that strong single-particle  $E1$  transitions would be facilitated from these resonances to low-lying positive-parity states of  $^{25}\text{Mg}$ , which have a large spectroscopic factor.

## II. EXPERIMENTS

Employing a time-of-flight (TOF) technique, we have observed gamma rays from neutron capture in the 84-keV  $p_{3/2}$ -wave resonance, 266-keV  $p_{1/2}$ -wave resonance, and 431-keV  $p_{3/2}$ -wave resonance in  $^{24}\text{Mg}$  that have a large reduced neutron width. The experimental arrangement is shown in Fig. 1.

Pulsed neutrons were produced from the  $^7\text{Li}(p,n)^7\text{Be}$  reaction by bombarding a Li-evaporated copper disk with the 1.5-ns bunched proton beam from the 3.2-MV Pelletron Accelerator of the Research Laboratory for Nuclear Reactors in the Tokyo Institute of Technology. The copper disk was cooled by a blower from outside to prevent lithium from being scattered and lost. The neutron target thickness was determined by measuring neutron TOF spectra, as described below. The typical proton-beam current was  $9 \mu\text{A}$  at the 2-MHz pulse repetition rate. Capture samples were disks of natural

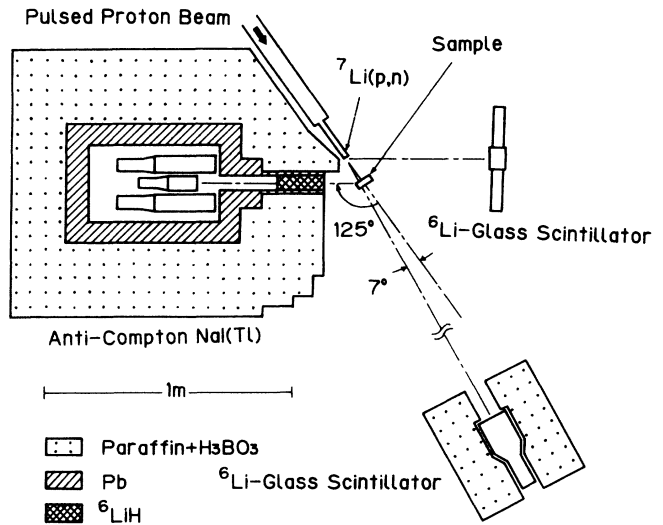


FIG. 1. Experimental arrangement.

magnesium, which were placed 156 mm away from the neutron source at right angles to the proton beam direction. The sample size was 60-mm in diameter by 2 mm for the 84-keV resonance experiment and 60-mm in diameter by 12 mm for the 266- and 431-keV resonance experiments. Here, we determined the sample thickness so as to give the neutron transmission of about 70% at the resonance peak, in order to make small the correction factor for neutron multiple scattering and self-shielding described in Sec. III B.

Capture gamma rays were detected with a 76-mm diameter by 152 mm NaI(Tl) detector, which was centered in a 254-mm diameter by 280 mm NaI(Tl) hollow anti-Compton detector surrounded by a heavy shield consisting of lead, cadmium, and borated paraffin.<sup>20</sup> The gamma-ray detector was located at a distance of 80 cm from the sample, with its axis at an angle of  $125^\circ$  to the proton-beam direction. Also, we inserted a 63-mm diameter by 300 mm metallic aluminum case filled with  $^6\text{LiH}$  powder in the gamma-ray collimator to remove the neutrons scattered into the detector from the sample. Since 70–80% of the background was caused by the neutrons coming through the collimator, the use of lithium-6 hydride extremely reduced the background that was produced mainly by neutron capture of iodine in the NaI(Tl) scintillator.<sup>21</sup> The response functions of the gamma-ray detector, which included the information on the detection efficiency and on the gamma-ray shielding effects of lithium-6 hydride, were determined with the aid of gamma rays from calibrated radioactive sources, an Am-Be neutron source, and the  $^{19}\text{F}(p,\alpha\gamma)^{16}\text{O}$  and  $^{27}\text{Al}(p,\gamma)^{28}\text{Si}$  reactions.<sup>22</sup>

Capture events detected by the gamma-ray detector were stored in a minicomputer as two-dimensional data on TOF and pulse height (PH). The background-subtracted data for the 84-keV resonance experiment are shown pictorially in Fig. 2, where the background was taken as being time independent and measured by setting a broad gate three times the gate of resonance capture gamma rays on the TOF spectrum.<sup>22</sup> The observed peaks

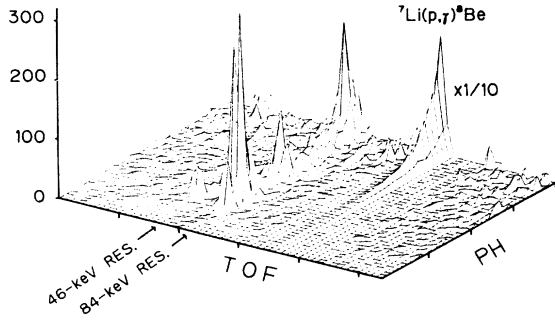


FIG. 2. Two-dimensional capture gamma-ray spectrum of TOF and PH obtained from the neutron capture experiment on  $^{24}\text{Mg}$  at neutron energies of  $E_n = 5\text{--}150\text{ keV}$ .

are due to gamma rays from the  $^7\text{Li}(p,\gamma)^8\text{Be}$  reaction and those from neutron capture in the 46-keV narrow resonance and 84-keV broad resonance.<sup>23</sup> The overall time resolution was 3.8 ns (FWHM) for gamma rays above 0.5 MeV, which was enough to unambiguously distinguish the 84-keV resonance peak from other peaks on the TOF spectrum, as seen from Fig. 2. This was the same in other resonance experiments. Thus, the gamma rays from the 84-keV resonance were obtained by setting a suitable TOF gate. In order to illustrate the signal to background ratio, we show in Fig. 3 the foreground and background gamma-ray pulse-height spectra for the 84-keV resonance experiment.

The capture cross section of  $^{24}\text{Mg}$  was determined by normalizing the capture gamma-ray yield of  $^{24}\text{Mg}$  to that of  $^{197}\text{Au}$ , which was related to the ENDF/B-V capture cross section of  $^{197}\text{Au}$  by means of a pulse-height weighting technique.<sup>24</sup> Therefore, measurements were performed alternately between the magnesium and gold sam-

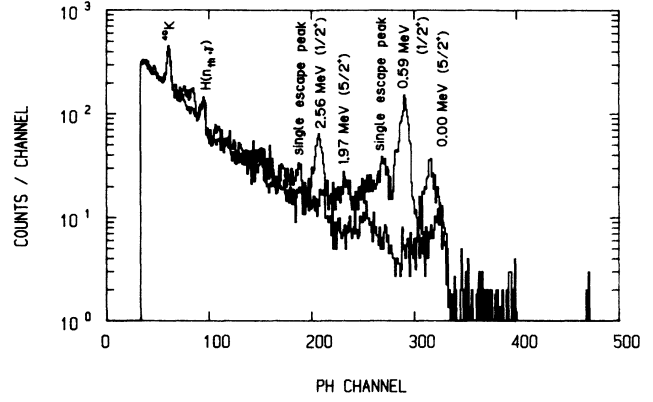


FIG. 3. Foreground and background gamma-ray pulse-height spectra in the 84-keV resonance experiment.

ple runs. Both data were normalized by neutron counts of the  $^6\text{Li}$ -glass scintillation detector, which was installed at an angle of  $45^\circ$  to the proton-beam direction so as to look directly at the neutron source.

Incident neutron spectra were measured without the sample, employing a 102-mm diameter by 6.4 mm  $^6\text{Li}$ -glass scintillation detector. The detector was placed at an angle of  $7^\circ$  to the proton-beam direction. The measurement at this angle gave approximately the averaged incident neutron spectrum on the sample. It was performed every 6 h in the Mg-sample run to take account of a change in the neutron spectrum shape. The energy dependence of the detection efficiency was calculated by a Monte Carlo method, using the cross section of the  $^6\text{Li}(n,\alpha)^3\text{H}$  reaction and considering the neutron multiple scattering on nuclei in the glass scintillator.<sup>25</sup> In Fig. 4, the neutron flux energy distributions normalized to one neutron are shown for the 84-keV, 266-keV, and 431-keV

TABLE I. Resonance parameters of the 84-, 257-, 266-, and 431-keV resonances.

$E_R$ (keV)	$J^\pi$	$\Gamma_n$ (keV)	$g\Gamma_n\Gamma_\gamma/\Gamma$ (eV)	Reference
83	$\frac{3}{2}^-$	$7.8\pm 0.5$		11
83.50	$\frac{3}{2}^-$	$7.6\pm 0.5$		12
83.5	$\frac{3}{2}^-$		$10\pm 2$	13
$83.50\pm 0.08$	$\frac{3}{2}^-$	$7.7\pm 0.5$	$9.3\pm 2^a$	15
257.2		$0.038\pm 0.005^b$	$2.32\pm 0.07$	13
$257.2\pm 0.3$	$l=2$	$0.038\pm 0.005^b$	$2.30\pm 0.07$	15
260	$\frac{1}{2}^-$	$75\pm 15$		11
265.2	$\frac{1}{2}^-$	$90\pm 5$		12
266	$\frac{1}{2}^-$	$78\pm 1$	$5.6\pm 4.5$	13
$266.0\pm 0.3$	$\frac{1}{2}^-$	$78\pm 1$	$5.2\pm 4.5$	15
426.3	$\frac{3}{2}^-$	$23.2\pm 2.3$		12
430.6	$\frac{3}{2}^-$	$31\pm 1$	$15\pm 2$	13
430.6	$\frac{3}{2}^-$	31		14
$430.6\pm 0.4$	$\frac{3}{2}^-$	$31\pm 1$	$14\pm 2$	15

<sup>a</sup>Reference 15 gives the value of  $93\pm 2$  eV. Probably it is a misprint for the value of  $9.3\pm 2$  eV.

<sup>b</sup>Values of  $g\Gamma_n$  are given because the resonance spin has never been assigned to this resonance.

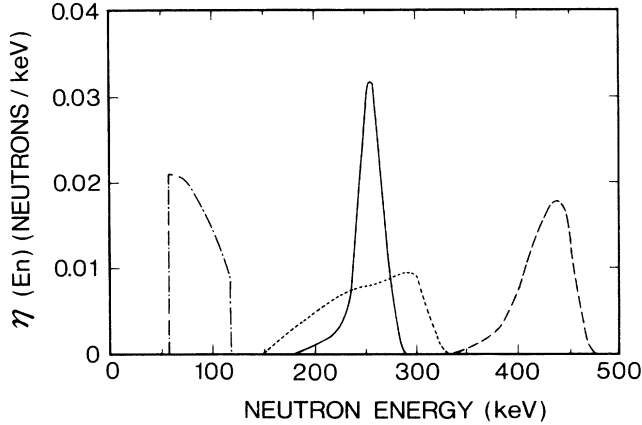


FIG. 4. Neutron flux energy distributions normalized to one neutron for the 84-keV (dash-dotted line), 431-keV (dashed line), and 266-keV (dotted and solid lines) resonance experiments.

resonance experiments. In the figure, the distribution for the 84-keV resonance experiment was obtained by normalizing the neutron energy spectrum within the TOF gate width, because monoenergetic neutrons were not available at this resonance energy. In the 266-keV resonance experiment, moreover, we took measurements using the neutron flux with the broad and narrow energy distributions in order to separate the contribution of the 257-keV narrow resonance overlapping with the 266-keV broad resonance. Resonance parameters of these resonances are given in Table I. The data are in good agreement with each other.

### III. EXPERIMENTAL RESULTS

#### A. Resonance capture gamma-ray spectra

Figures 5(a), 6(a), 7(a), and 8(a) show the pulse-height spectra of capture gamma rays measured using the neutron flux given in Fig. 4. In order to obtain gamma-ray energy spectra, these pulse-height spectra were unfolded by an iterative method<sup>26</sup> (see the Appendix), using the matrix represented by a product of the gamma-ray response matrix and correction matrix. The correction matrix was generated by a Monte Carlo method to take into account photoelectric absorption, Compton scattering, and pair creation of capture gamma rays in the sample. For reference, we show the gamma-ray attenuation factors  $C_\gamma$  of the sample in Table II, which are diagonal elements of the correction matrix. The correction was found to be several percent at most.

##### 1. 84-keV $p_{3/2}$ -wave resonance

As shown in Fig. 5(a), distinct gamma rays were observed for the  $E1$  transitions to the ground ( $\frac{5}{2}^+$ ), 585-keV ( $\frac{1}{2}^+$ ), 1965-keV ( $\frac{5}{2}^+$ ), and 2564-keV ( $\frac{1}{2}^+$ ) states in  $^{25}\text{Mg}$ . In addition to these transitions, a small gamma-ray peak at 6.4 MeV, which may be due to the transition to the 975-keV ( $\frac{3}{2}^+$ ) state, is found in the unfolded gamma-ray energy spectrum of Fig. 5(b). We note that

the  $E1$  transitions to the  $\frac{3}{2}^+$  states at 975 and 2801 keV are extremely weak or imperceptible, despite the large spectroscopic factor of both states. The 5474-keV ( $\frac{1}{2}^+$ ) state transition cannot be identified because the gamma-ray peak due to this transition is so close to the gamma-ray peak due to the cascade transition from the 2564-keV state to the 585-keV state.

On the other hand, strong  $M1$  transitions were expected to the 3414-keV ( $\frac{3}{2}^-$ ) and 4277-keV ( $\frac{1}{2}^-$ ) negative-parity states with considerable spectroscopic factor. However, no appreciable gamma-ray peak due to the 3414-keV state transition was observed; a very small peak at 3.15 MeV in the unfolded spectrum might be due to the 4277-keV state transition.

Moreover, cascade gamma-ray peaks, though not indicated in Figs. 5(a) and (b), are found corresponding to the transitions from the 2564-keV state to the ground, 585-keV, and 975-keV states, and the transitions from the 1965-keV state to the 585-keV and 975-keV states. If the

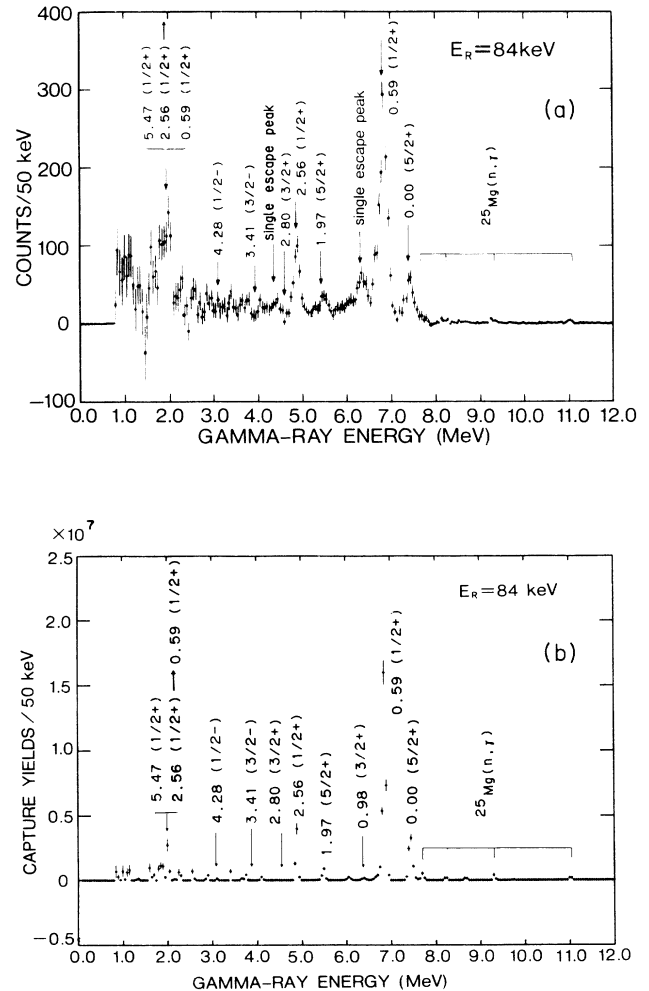


FIG. 5. (a) Capture gamma-ray pulse-height spectrum in the 84-keV resonance experiment. (b) Unfolded capture gamma-ray energy spectrum in the 84-keV resonance experiment.

gamma-ray peak at 1.97 MeV was produced only by the transition from the 2564-keV state to the 585-keV state, the branching ratio for this transition is  $0.62 \pm 0.29$ , which is in reasonable agreement with the previous value,  $0.80 \pm 0.01$ ,<sup>27</sup> within the experimental error.

In this experiment, the gamma-ray pulse-height spectrum was obtained by setting the TOF gate on the neutron energy region of 60–120 keV. In this energy region, seven neutron resonances in  $^{25}\text{Mg}$  have been observed.<sup>16</sup> Therefore, four gamma-ray peaks above 7.5 MeV would have been produced by the neutron capture in  $^{25}\text{Mg}$  leading to the ground ( $0^+$ ), 1809-keV ( $2^+$ ), 2938-keV ( $2^+$ ), and 3588-keV ( $0^+$ ) states. The ratio of these transition strengths is 1.0:1.6:1.0:2.8. No peak due to the 3941-keV ( $3^+$ ) state transition in  $^{26}\text{Mg}$  was observed at the expected gamma-ray energy of 7.23 MeV. Incidentally, the average partial neutron capture cross section for the ground state transition following neutron capture by  $^{25}\text{Mg}$  is  $5.1 \times 10^{-4} \pm 1.7 \times 10^{-4}$  barn.

## 2. 431-keV $p_{3/2}$ -wave resonance

The  $E1$  transitions to the ground ( $\frac{5}{2}^+$ ), 585-keV ( $\frac{1}{2}^+$ ), and 2564-keV ( $\frac{1}{2}^+$ ) states in  $^{25}\text{Mg}$  were identified, as shown in Fig. 6(a). In the unfolded spectrum in Fig. 6(b), two gamma-ray peaks around 6.8 MeV may have been produced by the transitions to the 975-keV ( $\frac{3}{2}^+$ ) state in  $^{25}\text{Mg}$ , the ground ( $\frac{1}{2}^+$ ) state in  $^{27}\text{Mg}$ , and the triplet ( $2^+, 4^+, 0^+$ ) states in  $^{26}\text{Mg}$  around the excitation energy of 4.9 MeV. The gamma-ray peak around 5.95 MeV would have been principally produced by the  $^{26}\text{Mg}(n, \gamma)^{27}\text{Mg}$  reaction, because the peak energy coincides with the gamma-ray energy for the 985-keV ( $\frac{3}{2}^+$ ) state transition in  $^{27}\text{Mg}$ . This peak may also include the gamma rays due to the 1965-keV ( $\frac{5}{2}^+$ ) state transition in  $^{25}\text{Mg}$ . Furthermore, a small gamma-ray peak is found at the gamma-ray energy for the 2801-keV ( $\frac{3}{2}^+$ ) state transition in  $^{25}\text{Mg}$ . However, we could not distinguish this peak from the gamma rays produced by the 1940-keV

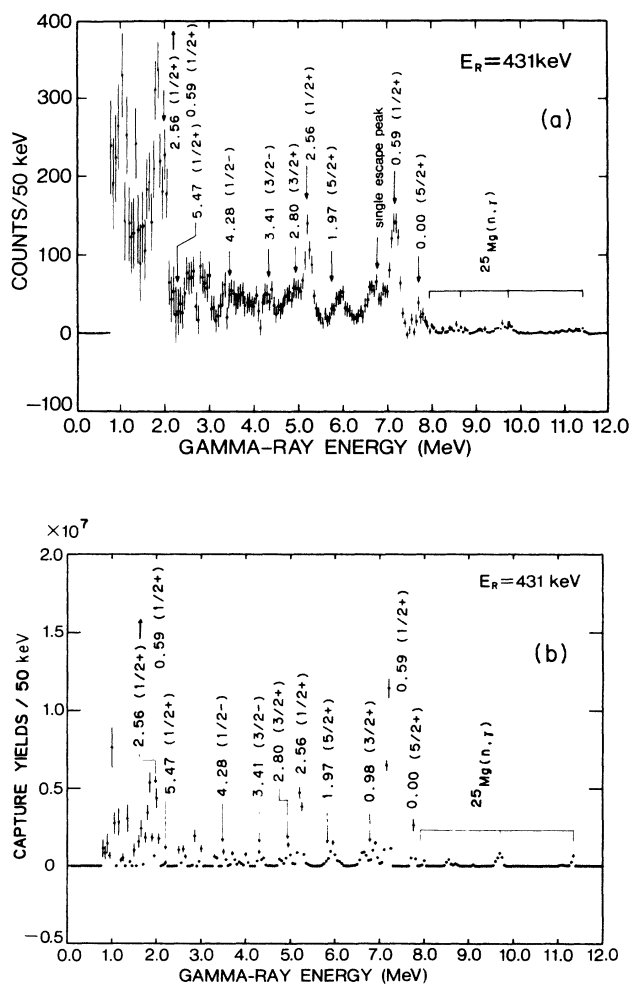


FIG. 6. (a) Capture gamma-ray pulse-height spectrum in the 431-keV resonance experiment. (b) Unfolded capture gamma-ray spectrum in the 431-keV resonance experiment.

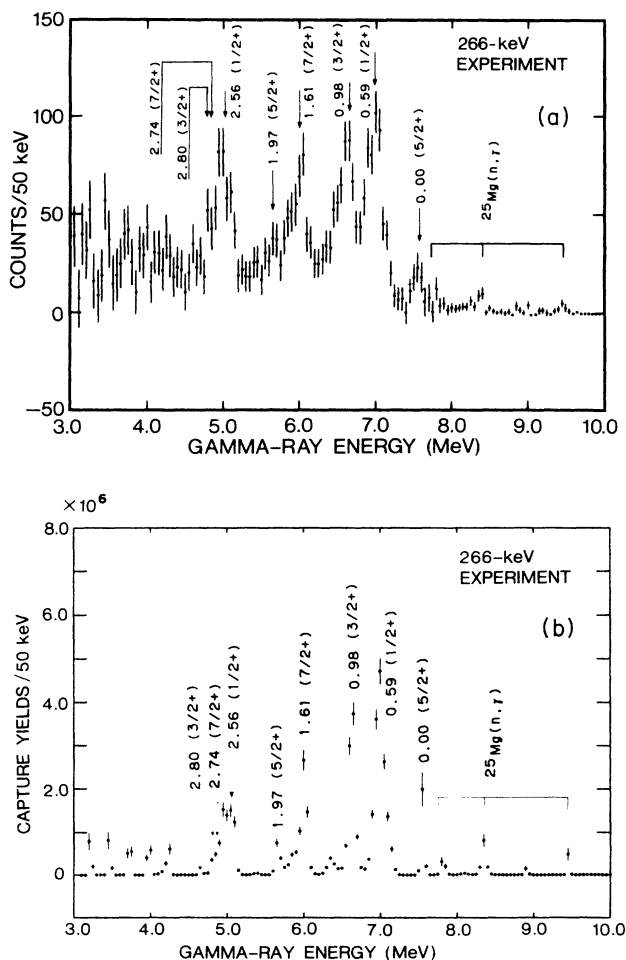


FIG. 7. (a) Capture gamma-ray pulse-height spectrum in the 266-keV experiment using the neutron flux shown by the dotted line in Fig. 4. (b) Unfolded capture gamma-ray energy spectrum in the 266-keV experiment using the neutron flux shown by the dotted line in Fig. 4.

( $\frac{5}{2}^+$ ) state transition in the  $^{26}\text{Mg}(n,\gamma)^{27}\text{Mg}$  reaction. An appreciable peak due to the 5474-keV ( $\frac{1}{2}^+$ ) state transition in  $^{25}\text{Mg}$  was observed at the expected gamma-ray energy of 2.27 MeV.

Weak transition strength was also observed at the gamma-ray energy of 4.33 MeV, corresponding to the  $M1$  transition to the 3414-keV ( $\frac{3}{2}^-$ ) negative-parity state. However, no appreciable peak due to the 4277-keV ( $\frac{1}{2}^-$ ) state transition was found at the expected gamma-ray energy of 3.47 MeV.

Moreover, a gamma-ray peak was identified for the cascade gamma-ray transition from the 2564-keV state to the 585-keV state. The branching ratio for this transition was deduced to be  $0.73 \pm 0.29$ . This value is in substantial agreement with the above mentioned value,  $0.80 \pm 0.01$ .

In the neutron energy region of this experiment, neutron resonances in  $^{25}\text{Mg}$  have been observed at 386, 423, 432, and 466 keV.<sup>16</sup> Therefore, the gamma-ray peaks above 7.8 MeV may have been produced by the neutron

capture in  $^{25}\text{Mg}$  leading to the ground ( $0^+$ ), 1809-keV ( $2^+$ ), 2938-keV ( $2^+$ ), and 3588-keV ( $0^+$ ) states. The ratio of these transition strengths is 1.0:1.8:0.8:0.3. No transition to the 3941-keV ( $3^+$ ) state in  $^{26}\text{Mg}$  was observed. Also, the average partial neutron capture cross section for the ground state transition following neutron capture by  $^{25}\text{Mg}$  is  $1.57 \times 10^{-4} \pm 0.20 \times 10^{-4}$  barn.

### 3. 266-keV $p_{1/2}$ -wave resonance

As seen from Table I, there is also the 257-keV narrow  $d$ -wave resonance in the vicinity of the 266-keV  $p_{1/2}$ -wave broad resonance. In order to separate these two resonances, an experiment was performed using the broad energy neutron flux (266-keV experiment) and narrow energy neutron flux (257-keV experiment) given in Fig. 4. Figures 7(a) and 8(a) show the gamma-ray pulse-height spectra obtained in both experiments. The unfolded spectra are given in Figs. 7(b) and 8(b).

In the 257-keV experiment, gamma-ray transitions from the  $d$ -wave resonance are emphasized in the gamma-ray spectrum, because the overlap of the broad  $p$ -wave resonance with the neutron energy distribution is more reduced than that in the 266-keV experiment. From a comparison between both gamma-ray spectra, we find that in the 257-keV experiment the 1612-keV ( $\frac{7}{2}^+$ ) state transition is relatively emphasized and the 585-keV ( $\frac{1}{2}^+$ ) state transition is relatively weakened, while these results are reversed in the 266-keV experiment. In other words, the  $\frac{7}{2}^+$  state transition is dominated by  $d$ -wave neutron capture and the  $\frac{1}{2}^+$  state transition by  $p$ -wave neutron capture, which appears to indicate that the spin of the 257-keV  $d$ -wave resonance is  $\frac{5}{2}$ .

### B. Partial radiative widths

The partial capture cross section of  $^{24}\text{Mg}$  averaged with a neutron flux distribution,  $\langle \sigma_{\gamma f}(\text{Mg}) \rangle$ , is related to the average total capture cross section of  $^{197}\text{Au}$ ,  $\langle \sigma_{\gamma}(\text{Au}) \rangle$ , as follows:

$$\langle \sigma_{\gamma f}(\text{Mg}) \rangle = CR \frac{\phi(\text{Au})}{\phi(\text{Mg})} \frac{N_{\gamma f}(\text{Mg})}{Y_{\gamma}(\text{Au})} \langle \sigma_{\gamma}(\text{Au}) \rangle \quad (1a)$$

with

$$C = \frac{(C_{nm} C_{ns})^{\text{Au}}}{(C_{nm} C_{ns})^{\text{Mg}}} \quad (1b)$$

and

$$R = \frac{(r^2 n)^{\text{Au}}}{(r^2 n)^{\text{Mg}}}, \quad (1c)$$

where  $r$  and  $n$  are the radius and thickness (atoms/b) of the sample, respectively;  $N_{\gamma f}(\text{Mg})$  is the partial capture yield for the transition to the state  $f$  in  $^{25}\text{Mg}$ , which was obtained by summing up the counts of the corresponding gamma-ray peak in the unfolded spectrum; and  $Y_{\gamma}(\text{Au})$  is the total capture yield of  $^{197}\text{Au}$ , which was obtained from the capture gamma-ray spectrum, using the pulse-height weighting technique.<sup>24</sup> The quantity,  $\phi$ , is the total neu-

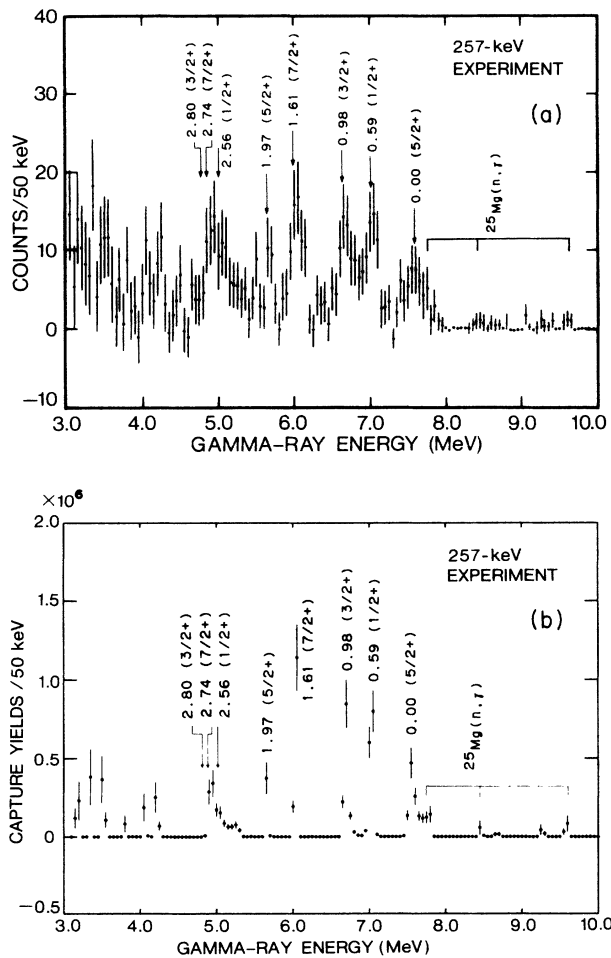


FIG. 8. (a) Capture gamma-ray pulse-height spectrum in the 257-keV experiment using the neutron flux shown by the solid line in Fig. 4. (b) Unfolded capture gamma-ray energy spectrum in the 257-keV experiment using the neutron flux shown by the solid line in Fig. 4.

TABLE II. Correction factors for neutron multiple scattering ( $C_{nm}$ ), for neutron selfshielding ( $C_{ns}$ ), and for gamma-ray attenuation ( $C_\gamma$ ) in the sample.

Resonance energy (keV)	Mg			Au		
	$C_{nm}$	$C_{ns}$	$C_\gamma$	$C_{nm}$	$C_{ns}$	$C_\gamma$
84	1.25	0.86	0.99	1.18	0.95	0.90–0.95
266 <sup>a</sup>	1.25	0.74	0.95–0.96	1.13	0.96	
266 <sup>b</sup>	1.51	0.75		1.13	0.96	
431	1.28	0.76		1.12	0.97	

<sup>a</sup>Correction factors for the experiment using the neutron flux shown by the solid line in Fig. 4.

<sup>b</sup>Correction factors for the experiment using the neutron flux shown by the dotted line in Fig. 4.

tron counts measured at an angle of 45° to the proton beam direction;  $C_{nm}$  is the correction factor for neutron multiple scattering, which was calculated by a Monte Carlo method, taking account of neutron scattering and capture in the sample;<sup>28</sup>  $C_{ns}$  is the correction factor for neutron selfshielding in the sample, which was calculated by means of the modified Schmitt formula.<sup>29</sup> Tables II and III show the correction factors and the thickness of the samples used in experiment, respectively. The average capture cross section,  $\langle\sigma_\gamma\rangle$ , was calculated as

$$\langle\sigma_\gamma\rangle = \int \sigma_\gamma(E)\eta(E)dE, \quad (2)$$

where  $\eta(E)$  is the normalized neutron energy distribution given in Fig. 4. The average capture cross section of <sup>197</sup>Au was calculated using the evaluated value of the ENDF/B-V data file.<sup>30</sup>

Since interference between resonance and off-resonance capture is neglected to a good approximation, the average partial capture cross section of <sup>24</sup>Mg,  $\langle\sigma_{\gamma f}(\text{Mg})\rangle$ , is connected to the partial radiative width,  $\Gamma_{\gamma f}$ :

$$\langle\sigma_{\gamma f}(\text{Mg})\rangle = \alpha\Gamma_{\gamma f} + \sigma_{\gamma f}(\text{off}) \quad (3a)$$

with

$$\alpha \equiv \int \pi\lambda^2(E)g \frac{\Gamma_n\eta(E)}{(E-E_R)^2 + (\Gamma/2)^2} dE, \quad (3b)$$

where  $g$  is a statistical factor and  $\lambda(E)$  is the de Broglie wavelength of the incident neutron with energy  $E$ . The resonance parameters,  $E_R$ ,  $\Gamma$ , and  $\Gamma_n$ , are the resonance energy, total width, and neutron width, respectively. In the present analysis, these parameters are taken from the work of Mughabghab *et al.*<sup>16</sup>

The partial off-resonance capture cross sections,  $\sigma_{\gamma f}(\text{off})$ , were calculated on the basis of the potential-capture theory,<sup>6</sup> using the computer code HIKARI.<sup>31</sup> This

TABLE III. Thickness of the magnesium and gold samples.

Resonance energy (keV)	Sample thickness (atoms/b)	
	Mg	Au
84	$6.78 \times 10^{-3}$	$1.02 \times 10^{-2}$
266	$4.06 \times 10^{-2}$	
431	$4.06 \times 10^{-2}$	

theory has successfully reproduced the partial off-resonance capture cross sections of <sup>16</sup>O measured at the neutron energy of 280 keV.<sup>1</sup> However, the calculations may include the error of 20–30% originating from the ambiguity in making a choice of the optical potential parameters used, because the potential capture cross section is sensitive to these parameters. Also, the partial capture cross sections of <sup>24</sup>Mg for thermal neutrons were in substantial agreement with the model calculations assuming single-particle transitions from the capture state.<sup>32</sup> Therefore, the above calculation of partial off-resonance capture cross sections of <sup>24</sup>Mg appears to be acceptable. However, these cross sections account for only 10% of the average partial capture cross sections,  $\langle\sigma_{\gamma f}(\text{Mg})\rangle$ .

The error of partial radiative widths was calculated, including the statistical error (2–30%), the error of the detection efficiency of gamma rays (3–9%), the error of the total capture yield of gold (5%), and the error of the capture cross section of gold (5%).

The observed partial radiative widths of the 84-keV  $p_{3/2}$ -wave resonance are compared in Table IV with the data of Bergqvist *et al.*<sup>17</sup> Since their original data were measured at an angle of 90°, the values given in the table were obtained from the correction of these original data, using the calculated gamma-ray angular distribution for  $E1$  transition. As seen from the table, our values are about twice as much as their values for all observed transitions. However, our value for the ground state transition is in general agreement with the value of Coeva *et al.*,  $\Gamma_{\gamma 0} = 0.78$  eV,<sup>33</sup> and with the value of Baglan *et al.*,  $\Gamma_{\gamma 0} = 1.1$  eV,<sup>34</sup> measured by the <sup>25</sup>Mg( $\gamma, n$ )<sup>24</sup>Mg reaction.

On the total radiative width,  $\Gamma_\gamma = 6.7 \pm 0.9$  eV was reported by Block *et al.*,<sup>35</sup>  $\Gamma_\gamma = 5 \pm 1$  eV by Weigmann *et al.*,<sup>14</sup>  $\Gamma_\gamma = 4.0 \pm 0.9$  eV by Nyström *et al.*,<sup>36</sup> and  $\Gamma_\gamma = 4.4 \pm 0.6$  eV by Allen *et al.*<sup>37</sup> The sum of our observed partial radiative widths,  $\sum\Gamma_{\gamma f} = 5.9 \pm 0.6$  eV, agrees well with these data.

The 431-keV resonance experiment produced partial radiative widths for the transitions to the ground ( $\frac{5}{2}^+$ ), 585-keV ( $\frac{1}{2}^+$ ) and 2564-keV ( $\frac{1}{2}^+$ ) states in <sup>25</sup>Mg, as given in Table V. In addition, for the reason mentioned in Sec. III A 2, only upper limits of partial radiative widths were deduced for the transitions to the 975-keV ( $\frac{3}{2}^+$ ), 1965-keV ( $\frac{5}{2}^+$ ), and the 2801-keV ( $\frac{3}{2}^+$ ) states. These upper limits were obtained at the gamma-ray energies of 6.77,

TABLE IV. Partial radiative widths of the 84-keV  $p_{3/2}$ -wave resonance.

$E_x$ (MeV)	Present	Partial radiative widths (eV)		$ e_{ren}/\bar{e} ^a$
		Bergqvist <sup>b</sup>	Valence	
0.00 ( $\frac{5}{2}^+$ )	0.93±0.14	0.60	2.78	0.58
0.59 ( $\frac{1}{2}^+$ )	3.98±0.57	1.88	4.31	0.96
0.98 ( $\frac{3}{2}^+$ )	<0.10		0.16	
1.97 ( $\frac{5}{2}^+$ )	0.20±0.03	0.081	0.44	0.67
2.56 ( $\frac{1}{2}^+$ )	0.68±0.11	0.35	0.69	0.99
2.80 ( $\frac{3}{2}^+$ )			0.08	
3.41 ( $\frac{3}{2}^-$ )				
4.27 ( $\frac{1}{2}^-$ )	<0.03			

<sup>a</sup>Renormalized effective charges are given in the unit of  $\bar{e} = -Ze/A$ .

<sup>b</sup>These values were obtained from the correction of the original data (Ref. 17), using the calculated gamma-ray angular distribution for E1 transition.

5.78, and 4.95 MeV by summing up the counts in the energy bin of 250 keV corresponding to the energy resolution of the gamma-ray detector. The upper limit for the 5474-keV ( $\frac{1}{2}^+$ ) state transition was obtained by summing up the counts in the energy bin of 150 keV at the gamma-ray energy of 2.27 MeV. Upper limits were obtained similarly for the transitions to both negative-parity states.

On the total radiative width of the 431-keV resonance,  $\Gamma_\gamma = 7.5 \pm 1.0$  eV was reported by Weigmann *et al.*<sup>14</sup> The summation of all observed partial radiative widths produces  $\sum \Gamma_{\gamma f} = 5.40 \pm 0.57$  eV. Since this value includes the upper limits of several partial radiative widths, the observed value of Weigmann *et al.* seems to be too large.

In order to obtain partial radiative widths of the 266-keV  $p_{1/2}$ -wave resonance, Eq. (3) must be modified to include the contribution of the 257-keV  $d$ -wave resonance. The total width of the 257-keV  $d$ -wave resonance is known to be very narrow; therefore the resonance integral is written

TABLE V. Partial radiative widths for the 431-keV  $p_{3/2}$ -wave resonance.

$E_x$ (MeV)	Partial radiative widths (eV)		$ e_{ren}/\bar{e} ^a$
	Present	Valence	
0.00 ( $\frac{5}{2}^+$ )	0.35±0.07	1.86	0.43
0.59 ( $\frac{1}{2}^+$ )	2.53±0.37	2.89	0.94
0.98 ( $\frac{3}{2}^+$ )	0.48±0.07 <sup>b</sup>	0.11	
1.97 ( $\frac{5}{2}^+$ )	0.25±0.03 <sup>b</sup>	0.31	
2.56 ( $\frac{1}{2}^+$ )	1.04±0.14	0.60	1.32
2.80 ( $\frac{3}{2}^+$ )	0.28±0.04 <sup>b</sup>	0.06	
3.41 ( $\frac{3}{2}^-$ )	<0.18		
4.27 ( $\frac{1}{2}^-$ )	<0.09		
5.47 ( $\frac{1}{2}^+$ )	<0.10	0.09	

<sup>a</sup>Renormalized effective charges are given in the unit of  $\bar{e} = -Ze/A$ .

<sup>b</sup>These values show the upper limit of partial radiative widths (see text).

$$2\pi^2\lambda^2(E'_R)\eta(E'_R)g' \frac{\Gamma'_n \Gamma'_{\gamma f}}{\Gamma'} . \quad (4)$$

Thus, instead of Eq. (3) the average capture cross section is expressed by the sum of the contributions of two resonances as

$$\langle \sigma_{\gamma f}^i \rangle = \alpha^i \Gamma_{\gamma f} + 2\pi^2\lambda^2(E'_R)\eta^i(E'_R)g' \frac{\Gamma'_n \Gamma'_{\gamma f}}{\Gamma'} + \sigma_{\gamma f}(\text{off}) , \quad (5)$$

where the superscript  $i$  distinguishes the 266-keV experiment from the 257-keV experiment, and the primed resonance parameters denote those of the 257-keV resonance. In Eq. (5), the first and second terms represent the contributions of the 266-keV and 257-keV resonances, respectively. Two different experiments generate two independent data sets of  $\alpha^i$ ,  $\eta^i(E'_R)$ , and  $\langle \sigma_{\gamma f}^i \rangle$ . As a result, the unknown variables,  $\Gamma_{\gamma f}$  and  $g'\Gamma'_n \Gamma'_{\gamma f}/\Gamma'$ , are determined from two equations for Eq. (5). In Table VI partial radiative widths are given for the transitions from the 266-keV resonance to the ground ( $\frac{5}{2}^+$ ), 585-keV ( $\frac{1}{2}^+$ ), 975-keV ( $\frac{3}{2}^+$ ), 1612-keV ( $\frac{7}{2}^+$ ), and 1965-keV ( $\frac{5}{2}^+$ ) states. Also, the 257-keV partial resonance kernels ( $\equiv g'\Gamma'_n \Gamma'_{\gamma f}/\Gamma'$ ) for the transitions to these states are given in Table VII. Since the transitions to the 2564-keV ( $\frac{1}{2}^+$ ), 2736-keV

TABLE VI. Partial radiative widths of the 266-keV  $p_{1/2}$ -wave resonance.

$E_x$ (MeV)	Partial radiative widths (eV)		
	Present	Valence	PRC
0.00 ( $\frac{5}{2}^+$ )	<0.07		
0.59 ( $\frac{1}{2}^+$ )	6.07±2.2	12.2	5.8
0.98 ( $\frac{3}{2}^+$ )	3.78±1.8	5.8	3.2
1.61 ( $\frac{7}{2}^+$ )	0.13±0.40		
1.97 ( $\frac{5}{2}^+$ )	0.03±0.18		
2.56 ( $\frac{1}{2}^+$ )		1.5	2.0
2.74 ( $\frac{7}{2}^+$ )	2.73±0.86		
2.80 ( $\frac{3}{2}^+$ )		3.0	0.6

TABLE VII. Partial resonance kernels of the 257-keV  $d$ -wave resonance.

$E_x$ (MeV)	Partial resonance kernels (eV)
0.00 ( $\frac{5}{2}^+$ )	$0.47 \pm 0.15$
0.59 ( $\frac{1}{2}^+$ )	$< 0.07$
0.98 ( $\frac{3}{2}^+$ )	$0.08 \pm 0.16$
1.61 ( $\frac{7}{2}^+$ )	$0.68 \pm 0.32$
1.97 ( $\frac{5}{2}^+$ )	$0.19 \pm 0.08$
2.56 ( $\frac{1}{2}^+$ )	$0.08 \pm 0.18$
2.74 ( $\frac{7}{2}^+$ )	
2.80 ( $\frac{3}{2}^+$ )	

( $\frac{7}{2}^+$ ) and 2801-keV ( $\frac{3}{2}^+$ ) states could not be separated, only the sum of the partial radiative widths or resonance kernels for these transitions is given.

As seen from Table VII, the partial resonance kernel for the transition from the 257-keV  $d$ -wave resonance to the 585-keV ( $\frac{1}{2}^+$ ) state is nearly zero. Also, this resonance has the large kernel for the 1612-keV ( $\frac{7}{2}^+$ ) state transition. Therefore, the spin of this resonance may be  $\frac{5}{2}$ , as predicted in Sec. III A 3.

On the total radiative width of the 266-keV resonance,  $\Gamma_\gamma = 5.6 \pm 4.5$  eV was reported by Weigmann *et al.*<sup>14</sup> The sum of the observed partial radiative widths is  $\sum \Gamma_{\gamma f} = 12.5 \pm 4.2$  eV, which agrees with their value within the error.

$$\Gamma_{\gamma f} = \Gamma_n \left[ \frac{16\pi}{9\hbar} k_\gamma^3 \bar{e}^2 \theta_f^2 \right] \left[ \frac{1}{\text{Im} \tan \delta(\text{opt})} \text{Im} \int_0^\infty u_f r u_E(\text{opt}) dr \right]^2 \times \frac{3}{4\pi} (2J_f + 1)(2j_i + 1)(2j_f + 1)(2l_i + 1) [(l_i 0 1 0 | l_f 0) W(l_i j_i l_f j_f; \frac{1}{2} 1) W(j_i J_i j_f J_f; I 1)]^2, \quad (6)$$

where  $\Gamma_n$  is the neutron width,  $k_\gamma$  is the wave number of gamma rays,  $\bar{e}$  is the neutron effective charge ( $-Ze/A$ ), and  $\theta_f^2$  is the spectroscopic factor of a final state. The quantity  $I$  is the target spin,  $J$  is the spin of a nuclear state,  $j$  is the total spin of a neutron single-particle state, and  $l$  is the orbital angular momentum. The geometrical factors, Clebsch-Gordan coefficient ( $abcd|ef$ ) and Racah coefficient  $W(abcd;ef)$ , are produced by the vector coupling of spin and orbital angular momentum. The subscripts  $i$  and  $f$  denote the initial (resonance) and final states, respectively. The initial-state wave function,  $u_E(\text{opt})$ , is the optical-model solution, which has the asymptotic form

$$u_E(\text{opt}) \underset{r \rightarrow \infty}{\sim} \frac{1}{v^{1/2}} \left[ \sin(kr - \frac{1}{2}l_i\pi) + \tan \delta(\text{opt}) \cos(kr - \frac{1}{2}l_i\pi) \right], \quad (7)$$

where  $k$  is the wave number of an incident neutron with velocity,  $v$ , and  $\delta(\text{opt})$  is the optical-model phase shift. Moreover, the real central potential depth in the optical

#### IV. CALCULATIONS AND DISCUSSION

As seen from a comparison between Tables IV and V, the 84-keV and 431-keV  $p_{3/2}$ -wave resonances are very similar in the intensity distribution for the transitions to the ground ( $\frac{5}{2}^+$ ), 585-keV ( $\frac{1}{2}^+$ ), and 2564-keV ( $\frac{1}{2}^+$ ) states in  $^{25}\text{Mg}$ . In the framework of the nuclear statistical model, such a similarity is unexpected for two resonances with the same spin and parity, because in this model the partial reduced radiative width follows the Porter-Thomas distribution. Furthermore, it is found that the intensity of primary  $E1$  transitions from the 84-keV resonance depends on the spectroscopic factor of final states, except that the transitions to the  $\frac{3}{2}^+$  states are strikingly weakened in spite of the considerable spectroscopic factor of these states. These features are explained by the valence capture model, which assumes a single-particle transition for neutron resonance capture. That is to say, they originate from the fact that the model formula produces the partial radiative width proportional to the spectroscopic factor, while the geometrical factor in the formula, generated by the vector coupling of angular momentum, is extremely small for the  $p_{3/2} \rightarrow d_{3/2}$  transition.

From these considerations, we calculated partial radiative widths for  $E1$  transition using the computer code VALENCE,<sup>38</sup> which was programmed on the base of the Lane-Mughabghab valence-capture model,<sup>7</sup> and compared them with the observed values. According to this model, the partial radiative width,  $\Gamma_{\gamma f}$ , for  $E1$  transition is written

potential was adjusted so that the gradient of the real part of the wave function became zero at the nuclear surface, because the initial state is in resonance:

$$\left. \frac{d \text{Re}[u_E(\text{opt})]}{dr} \right|_{r=R} = 0. \quad (8)$$

The final-state wave function,  $u_f(r)$ , was obtained using a Wood-Saxon potential searched so as to reproduce the observed neutron binding energy. In the calculation of these wave functions, other potential parameters were taken from the work of Moldauer.<sup>39</sup> The optical potential parameters used in the calculation of the resonance state wave functions are given in Table VIII. However, it is known that the valence model calculations scarcely depend on the optical potential, especially on the imaginary term of the central potential.<sup>40</sup>

The partial radiative width in Eq. (6) is proportional to the neutron width and spectroscopic factor. As shown in Table I, the observed neutron widths are in agreement with each other within the uncertainty of 20%. In the

TABLE VIII. Optical potential parameters used in the calculation of the resonance state wave function.

Resonances	$V_0$ (MeV)	$W_s$ (MeV)	$V_{so}$ (MeV)	$R$ (fm)	$a$ (fm)	$b$ (fm)
$p_{3/2}$ wave	46	7	7	$1.16 A^{1/3} + 0.6$	0.62	1.0
$p_{1/2}$ wave	50	7	7	$1.16 A^{1/3} + 0.6$	0.62	1.0

present analysis, therefore, the values were taken from the work of Mughabghab *et al.*<sup>16</sup> Table IX shows the spectroscopic factors of nuclear states in  $^{25}\text{Mg}$ , in which the experimental values were obtained from the  $^{24}\text{Mg}(d,p)^{25}\text{Mg}$  reaction and the theoretical values from rotational model and shell-model calculations. As shown in the table, Meurders *et al.*<sup>41</sup> have measured spectroscopic factors up to a higher excited state. However, because their value for the ground state is 0.53, rather larger than other experimental and theoretical values, we used the recommended values of Endt<sup>46</sup> for the present calculation. The spectroscopic factor of the 5470-keV ( $\frac{1}{2}^+$ ) state was taken from the work of Meurders *et al.*

A comparison between the observed and calculated partial radiative widths is made in Tables IV and V. We notice an interesting fact that the observed and calculated values for the transitions to the  $\frac{1}{2}^+$  states are in general agreement; however, the observed values for the transitions to the  $\frac{5}{2}^+$  states (probably those for the  $\frac{3}{2}^+$ -state transitions as well) are systematically much smaller than the calculated values, i.e., only 20–50 % of these values. The essential difference between these two transition modes may be clarified by examining the details of transition-matrix elements.

Figures 9(a) and 9(b) show radial matrix elements for the valence-capture transitions to the ground state ( $1d_{5/2}$ ) and 585-keV state ( $2s_{1/2}$ ), respectively. In the figures, while the nuclear internal part of the matrix element for the  $2s_{1/2}$ -state transition is strongly cancelled, such a cancellation is not found for the  $1d_{5/2}$ -state transition [see overlap integrands in Figs. 9(a) and (b)]. It is conceivable that the  $d$ -state transition is coupled to the

$E1$  giant resonance that has the large 1p-1h amplitude in the nuclear internal region, while the  $s$ -state transition is almost decoupled from the giant resonance. Therefore, the valence-capture model calculation for the  $d$ -state transition needs a renormalization of the neutron effective charge.

The above-mentioned retardation of  $E1$  transition is well known for transitions between low-lying bound states. In neutron resonance capture reactions, however, such an obvious retardation of  $E1$  transitions to  $d$ -states has never been observed. In the last column of Tables IV and V, we show renormalized neutron effective charges derived from a comparison between the observed and calculated radiative widths. The  $l$ -independent expression for the  $E1$  effective charge proposed by Bohr and Mottelson<sup>3</sup> produces the renormalized  $E1$  charge of  $\sim 0.3$ , which is somewhat smaller than those obtained in this analysis.

On the other hand, as mentioned in Secs. III A 1 and III A 2, no appreciable strength has been observed for primary  $M1$  transitions to negative-parity states with large spectroscopic factor. This result differs sharply from strong  $M1$  transitions from broad  $s$ -wave neutron resonances in  $sd$ -shell nuclei.<sup>1</sup> In the  $s$ -wave resonance capture, it was shown that the enhancement of primary  $M1$  transitions is closely connected to the  $1^+$  core excitation in the resonance state. In the broad  $p$ -wave resonance capture, however, it is inconceivable that the large component of the possible  $1^+$  core-excitation configurations, ( $1^+ \otimes p_{3/2}$ ) and ( $1^+ \otimes p_{1/2}$ ), are mixed in the resonance. The reason is that the large  $M1$  strength in  $^{24}\text{Mg}$  has been observed at excitation energies above 10

TABLE IX. Spectroscopic factors of the nuclear levels in  $^{25}\text{Mg}$ .

$E_x$ (MeV)	$^{24}\text{Mg}(d,p)$ experiments			Refs. 41 and 44	Theory			Evaluation Ref. 46
	Ref. 41	Ref. 42	Ref. 43		Ref. 45	Ref. 43	Ref. 41	
0.00 ( $\frac{5}{2}^+$ )	0.53	0.18–0.44	0.37	0.33	0.33	0.33	0.32	0.37±0.08
0.59 ( $\frac{1}{2}^+$ )	0.49	0.46–0.83	0.25	0.17	0.44	0.28	0.44	0.51±0.07
0.98 ( $\frac{3}{2}^+$ )	0.37	0.19–0.48	0.24	0.29	0.18	0.23	0.22	0.35±0.07
1.97 ( $\frac{5}{2}^+$ )	0.10	0.06–0.15	0.07	0.08	0.07	0.09	0.08	0.11±0.02
2.56 ( $\frac{1}{2}^+$ )	0.16	0.12–0.20	0.09	0.56	0.35	0.47	0.16	0.13±0.02
2.80 ( $\frac{3}{2}^+$ )	0.31	0.21–0.50	0.44	0.17	0.32	0.25	0.27	0.36±0.07
3.41 ( $\frac{3}{2}^-$ )	0.30		0.33	0.22	0.08	0.22		0.26±0.05
3.97 ( $\frac{7}{2}^-$ )			0.40	0.14	0.20	0.11		0.51±0.09
4.27 ( $\frac{1}{2}^-$ )	0.21		0.20	0.05		0.01		0.19±0.03
5.47 ( $\frac{1}{2}^+$ )	0.17							

MeV (Ref. 47), and the centroid of neutron single-particle  $p$ -state components in  $^{25}\text{Mg}$  may be located at an excitation energy above 4 MeV; consequently the excitation energies of these configuration states ( $>14$  MeV) are apparently much higher than the  $p$ -wave resonance energies

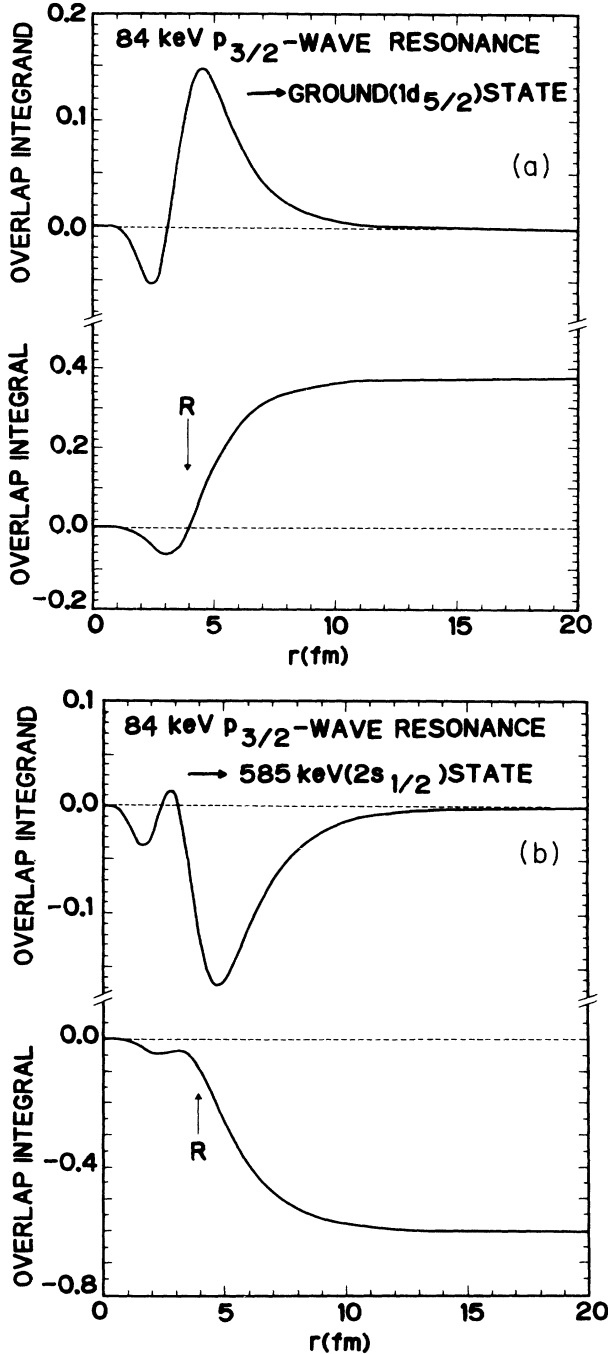


FIG. 9. (a) Radial overlap integral and integrand of the matrix element for the valence capture transition from the 84-keV  $p_{3/2}$ -wave resonance to the ground state.  $R$  stands for the nuclear radius of  $^{24}\text{Mg}$ . (b) Radial overlap integral and integrand of the matrix element for the valence capture transition from the 84-keV  $p_{3/2}$ -wave resonance to the 585-keV state.  $R$  stands for the nuclear radius of  $^{24}\text{Mg}$ .

in the weak coupling limit.

For the 266-keV  $p_{1/2}$ -wave resonance, the feature of primary capture gamma-ray transitions seems to be quite different from that for the  $p_{3/2}$ -wave resonances. In Table VI, the partial radiative widths for the 585-keV ( $\frac{1}{2}^+$ ) and 985-keV ( $\frac{3}{2}^+$ ) state transitions are about half of the valence model calculations, and so the particular retardation of  $E1$  transition is not found for the  $d_{3/2}$ -state transition. Taking account of the fact that the  $p_{3/2}$ -wave resonance capture is successfully explained by the valence capture model, the discrepancy between experiment and theory seems to be caused by the core excitation in the resonance state. Therefore, the core excitation in the resonance state and final states was explicitly considered for this resonance capture.

It is well known that the  $^{24}\text{Mg}$  nucleus is prolately deformed, and the ground ( $0^+$ ), 1369-keV ( $2^+$ ) and 4123-keV ( $4^+$ ) states in  $^{24}\text{Mg}$  belong to the ground rotational band. On the nucleus  $^{25}\text{Mg}$ , Litherland *et al.*<sup>45</sup> have shown that the structure of low-lying levels and the strength of  $E2$  transitions between these levels are described accurately by a rotational model. Also, in this mass region, the energy interval of collective states is comparable to that of single-particle states. In this analysis, therefore, the  $1d$ -,  $2s$ -,  $1f$ -, and  $2p$ -neutron single-particle states were nonadiabatically coupled to the member states belonging to the ground rotational band of  $^{24}\text{Mg}$  in order to obtain the wave functions of the resonance state and low-lying states in  $^{25}\text{Mg}$ .

The wave functions were searched so as to reproduce observed neutron binding energies, using the JUPITOR code<sup>48</sup> modified to solve the coupled-channel Schrödinger equation for bound states. The resonance state wave function was then approximated by a wave function of the state loosely bound at  $E_b=0.5$  MeV, the continuum nature of the wave function being neglected. Because it appears to be not largely different from the wave function obtained slightly above the neutron threshold, the approximation may be reasonable. In fact, it was confirmed that the configuration mixing amplitude scarcely changes for neutron binding energies,  $E_b=0.1-0.5$  MeV. In our calculation, the geometrical parameters of the real potential were cited from the work of Moldauer,<sup>39</sup> and the deformation parameters were taken to be  $\beta_2=0.48$  and  $\beta_4=-0.02$ .<sup>44</sup> The Wood-Saxon potential depth was searched in the energy region of 40–67 MeV so that it may not deviate greatly from observed optical potentials, because the potential depth cannot be determined uniquely for a given neutron-binding energy.

Consequently, four eigenfunctions for the resonance state were found using the base functions, ( $0^+ \otimes p_{1/2}$ ), ( $2^+ \otimes f_{5/2}$ ), ( $2^+ \otimes p_{3/2}$ ), and ( $4^+ \otimes f_{7/2}$ ). However, since the  $f_{5/2}$ -neutron single-particle component has never been observed for the  $^{24}\text{Mg}(d,p)^{25}\text{Mg}$  reaction, the configuration component ( $2^+ \otimes f_{5/2}$ ) in the resonance state is probably very small. Similarly, the configuration component ( $4^+ \otimes f_{7/2}$ ) would be small, because the  $4^+$  core-excited state is coupled very weakly to the  $0^+$  core-ground state. For the 266-keV  $p_{1/2}$ -wave resonance state, therefore, we chose the eigenfunction

$$\Psi_i(p_{1/2}) = \sqrt{0.33}(0^+ \otimes p_{1/2}) + \sqrt{0.04}(2^+ \otimes f_{5/2}) + \sqrt{0.51}(2^+ \otimes p_{3/2}) + \sqrt{0.12}(4^+ \otimes f_{7/2}). \quad (9)$$

Furthermore, some eigenfunctions were obtained for each of low-lying states in  $^{25}\text{Mg}$ . From these eigenfunctions, the function reproducing most reasonably the observed spectroscopic factor was chosen. Thus, the wave functions were obtained for four low-lying states in  $^{25}\text{Mg}$ :

$$\Psi_f(0.59, \frac{1}{2}^+) = -\sqrt{0.44}(0^+ \otimes s_{1/2}) - \sqrt{0.43}(2^+ \otimes d_{5/2}) - \sqrt{0.13}(2^+ \otimes d_{3/2}), \quad (10)$$

$$\begin{aligned} \Psi_f(0.98, \frac{3}{2}^+) = & -\sqrt{0.27}(0^+ \otimes d_{3/2}) - \sqrt{0.003}(2^+ \otimes d_{5/2}) \\ & + \sqrt{0.02}(2^+ \otimes d_{3/2}) - \sqrt{0.52}(2^+ \otimes s_{1/2}) + \sqrt{0.18}(4^+ \otimes d_{5/2}), \end{aligned} \quad (11)$$

$$\Psi_f(2.56, \frac{1}{2}^+) = \sqrt{0.26}(0^+ \otimes s_{1/2}) - \sqrt{0.33}(2^+ \otimes d_{5/2}) + \sqrt{0.41}(2^+ \otimes d_{3/2}), \quad (12)$$

and

$$\Psi_f(2.80, \frac{3}{2}^+) = \sqrt{0.43}(0^+ \otimes d_{3/2}) - \sqrt{0.01}(2^+ \otimes d_{5/2}) - \sqrt{0.18}(2^+ \otimes d_{3/2}) - \sqrt{0.03}(2^+ \otimes s_{1/2}) + \sqrt{0.35}(4^+ \otimes d_{5/2}). \quad (13)$$

Using the wave functions obtained above, we calculated partial radiative widths for  $E1$  transition as<sup>10</sup>

$$\Gamma_{\gamma f} = \frac{16\pi}{9} k_\gamma^3 \sum_{M_f, m} |\langle \Psi_{J_f M_f} | \epsilon_{1m}^\dagger | \Psi_{J_i M_i} \rangle|^2, \quad (14)$$

where  $\Psi_{J_i M_i}$  and  $\Psi_{J_f M_f}$  are the resonance state and final state wave functions, respectively. Using the neutron effective charge,  $\bar{e} = -Ze/A$ , the  $E1$  operator is written

$$\epsilon_{1m} = \bar{e} r Y_{1m}(\Omega). \quad (15)$$

In Table VI, the observed partial radiative widths of the 266-keV  $p_{1/2}$ -resonance are compared with valence-capture model and particle-rotator coupling model calculations (PRC). As seen from the table, the particle-rotator coupling model calculations reproduce quite accurately the observed widths. In particular, a great improvement in agreement between theory and experiment was made for the 585-keV ( $\frac{1}{2}^+$ ) state transition. For this transition, the valence component  $[(0^+ \otimes p_{1/2}) \rightarrow (0^+ \otimes s_{1/2})]$ , which is one dominant component in the particle-rotator coupling model calculation, produces the large partial radiative width of 13 eV. However, another dominant core-excitation component  $[(2^+ \otimes p_{3/2}) \rightarrow (2^+ \otimes d_{5/2})]$  is added destructively to the valence component, and consequently the model calculation reproduces the observed value. For the 975-keV ( $\frac{3}{2}^+$ ) state transition, the core-excitation component  $[(2^+ \otimes p_{3/2}) \rightarrow (2^+ \otimes s_{1/2})]$  is dominant, and the valence component  $[(0^+ \otimes p_{1/2}) \rightarrow (0^+ \otimes d_{3/2})]$  and core-excitation component  $[(4^+ \otimes f_{7/2}) \rightarrow (4^+ \otimes d_{5/2})]$  are added destructively to this dominant component.

Moreover, although we could not experimentally distinguish the 2564-keV ( $\frac{1}{2}^+$ ), 2740-keV ( $\frac{7}{2}^+$ ), and 2801-keV ( $\frac{3}{2}^+$ ) state transitions, the model calculations indicate the dominant transition to the 2564-keV ( $\frac{1}{2}^+$ ) state. This result is also supported by the observed gamma-ray spectrum shown in Fig. 7(b).

## V. SUMMARY

We have observed that primary  $E1$  transitions to the low-lying  $\frac{1}{2}^+$ ,  $\frac{3}{2}^+$ , and  $\frac{5}{2}^+$  states in  $^{25}\text{Mg}$  are facilitated

from the 84-keV and 431-keV  $p_{3/2}$ -wave resonances and 266-keV  $p_{1/2}$ -wave resonance with large reduced neutron width.

Consequently, it was found that the  $E1$  transitions from the  $p_{3/2}$ -wave resonances are successfully explained by the Lane-Mughabghab valence-capture model. However, the  $\frac{5}{2}^+$ -state transitions (probably the  $\frac{3}{2}^+$ -state transitions as well) are systematically retarded because of the coupling between the neutron single-particle transition and the  $E1$  field produced by GDR. Therefore, the model calculations for these transitions require the use of the renormalized  $E1$  effective charge for neutrons. Moreover, we found that a good agreement with the model calculations for the  $\frac{1}{2}^+$ -state transitions is due to the decoupling of the single-particle transitions from GDR, which originates from the strong cancellation of the transition matrix element in the nuclear internal region.

On the other hand, the observed  $E1$  transitions from the 266-keV  $p_{1/2}$  resonance are entirely different from the predictions of the valence-capture model. In order to remove the discrepancy, we proposed a particle-rotator coupling model, which took account of the core excitation in the resonance state. In this model, the  $1d$ -,  $2s$ -,  $1f$ -, and  $2p$ -neutron single-particle orbits were nonadiabatically coupled to the member states ( $0^+$ ,  $2^+$ , and  $4^+$ ) of the ground rotational band in  $^{24}\text{Mg}$ . As a result, an excellent agreement was obtained between experiment and theory.

## APPENDIX: ITERATIVE UNFOLDING METHOD

In this method,<sup>26</sup> a suitable gamma-ray energy spectrum  $f_j$  ( $j=1, 2, \dots, n$ ) is searched so as to maximize the quantity based on the Poisson distribution,  $\Lambda(f_j)$ :

$$\max \Lambda(f_j) = \max \prod_{i=1}^n \exp(-g_i) \frac{(g_i)^{p_i}}{p_i} \quad (A1a)$$

with

$$p_i = \sum_{j=1}^n k_{ij} f_j, \quad (A1b)$$

where  $g_i$  ( $i=1, 2, \dots, m$ ) is the observed gamma-ray

pulse-height spectrum and  $k_{ij}$  ( $i=1,2,\dots,m$ ;  $j=1,2,\dots,n$ ) is the response matrix of a gamma-ray detector.

In searching the spectrum  $f_j$ , it is effective to use the iterative scheme

$$f_j(n+1) = f_j(n) \frac{1}{\sum_{i=1}^m k_{ij}} \sum_{i=1}^m \frac{g_i k_{ij}}{\sum_{j=1}^n k_{ij} f_j(n)}, \quad (\text{A2})$$

where  $f_j(n)$  is the result of the  $n$ th iteration. Usually, the initial value of  $f_j$  is taken to be constant. In the present study, we made an initial guess of  $f_j$  to be  $1 \times 10^5$ . Here, we assumed a condition of convergence of the iterative calculation as

$$\left| \frac{\Lambda(f_j(n+1)) - \Lambda(f_j(n))}{\Lambda(f_j(n+1))} \right| \leq 10^{-5}. \quad (\text{A3})$$

The statistical error of  $f_j$  was calculated with the expression

$$\Delta f_j^2 = \sum_{i=1}^m \left[ \frac{\partial f_j}{\partial g_i} \right]^2 (\Delta g_i)^2, \quad (\text{A4})$$

where  $\partial f_j / \partial g_i$  was derived from Eq. (A2), and  $\Delta g_i$  is the statistical error for the  $i$ th channel of the observed gamma-ray pulse-height spectrum. The covariance of  $\Delta g_i$  and  $\Delta g_k$  ( $i \neq k$ ) was assumed to be zero.

Thus, we obtained unfolded spectra with sharp peaks of capture gamma rays, as shown in Figs. 5(b), 6(b), 7(b), and 8(b). Smoothing of the unfolded gamma-ray spectrum was quite unnecessary for removing the oscillation of the spectrum.

- <sup>1</sup>H. Kitazawa and M. Igashira, in *Proceedings of the Sixth International Symposium on Capture Gamma-Ray Spectroscopy, Leuven, Belgium, 1987*, Inst. Phys. Conf. Series No. 88, edited by K. Abrahams and P. Van Assche (Institute of Physics, Bristol, U.K., 1988), p. S215; J. Phys. G **14**, S215 (1988).
- <sup>2</sup>M. Shimizu, M. Igashira, K. Terazu, and H. Kitazawa, Nucl. Phys. **A452**, 205 (1986).
- <sup>3</sup>A. Bohr and B. R. Mottelson, *Proceedings of the International Symposium on Neutron Gamma-Ray Spectroscopy, Studsvik, Sweden, 1969* (IAEA, Vienna, 1969), p. 3.
- <sup>4</sup>B. Gyarmati, A. M. Lane, and J. Zimányi, Phys. Lett. **50B**, 316 (1974).
- <sup>5</sup>M. Harvey and F. C. Khanna, Nucl. Phys. **A221**, 77 (1974).
- <sup>6</sup>A. M. Lane and J. E. Lynn, Nucl. Phys. **17**, 563 (1960).
- <sup>7</sup>A. M. Lane and S. F. Mughabghab, Phys. Rev. C **10**, 412 (1974).
- <sup>8</sup>William P. Beres and M. Divadeenam, Phys. Rev. Lett. **25**, 596 (1970).
- <sup>9</sup>D. Halderson, B. Castel, M. Divadeenam, and H. W. Newson, Ann. Phys. (N.Y.) **103**, 133 (1977).
- <sup>10</sup>H. Kitazawa, M. Ohgo, T. Uchiyama, and M. Igashira, Nucl. Phys. **A464**, 61 (1987).
- <sup>11</sup>B. J. Allen, A. R. de L. Musgrove, R. L. Macklin, and R. R. Winters, in *Proceedings of a Specialist's Meeting on Neutron Data of Structural Materials for Fast Reactors, Geel, Belgium, 1977*, edited by K. H. Böckhoff (Pergamon, New York, 1978), p. 506.
- <sup>12</sup>H. W. Newson, R. C. Block, P. F. Nichols, A. Taylor, and A. K. Furr, Ann. Phys. (N.Y.) **8**, 211 (1959).
- <sup>13</sup>U. N. Singh, H. I. Liou, J. Rainwater, G. Hacken, and J. B. Garg, Phys. Rev. C **10**, 2150 (1974).
- <sup>14</sup>H. Weigmann, R. L. Macklin, and J. A. Harvey, Phys. Rev. C **14**, 1328 (1976).
- <sup>15</sup>D. J. Horen, J. A. Harvey, and N. W. Hill, Phys. Rev. C **15**, 1168 (1977).
- <sup>16</sup>S. F. Mughabghab, M. Divadeenam, and N. E. Holden, *Neutron Cross Sections* (Academic, New York, 1981), Vol. 1., p. 12-2.
- <sup>17</sup>I. Bergqvist, J. A. Biggerstaff, J. H. Gibbons, and W. M. Good, Phys. Rev. **158**, 1049 (1967).
- <sup>18</sup>A. M. Lane, in *Proceedings of the International Conference on Photonuclear Reactions and Applications, Asilomar, California, 1973*, edited by B. L. Berman (U.S. Atomic Energy Commission Office of Information Services, Oak Ridge, Tennessee, 1973), Vol. 2, p. 803.
- <sup>19</sup>S. F. Mughabghab, in *Proceedings of the International Conference on Photonuclear Reactions and Applications, Asilomar, California, 1973*, edited by B. L. Berman (U.S. Atomic Energy Commission Office of Information Services, Oak Ridge, Tennessee, 1973), Vol. 1, p. 301.
- <sup>20</sup>M. Igashira, H. Kitazawa, and N. Yamamuro, Nucl. Instrum. Methods **A245**, 432 (1986).
- <sup>21</sup>M. Shimizu, PhD. thesis, Tokyo Institute of Technology, 1985.
- <sup>22</sup>M. Igashira, H. Kitazawa, M. Shimizu, H. Komano, and N. Yamamuro, Nucl. Phys. **A457**, 301 (1986).
- <sup>23</sup>T. Uchiyama, M. Igashira, and H. Kitazawa, in *Proceedings of the International Conference on Nuclear Data for Science and Technology, Mito, Japan, 1988*, edited by S. Igarasi (Saikon, Tokyo, 1988), p. 733.
- <sup>24</sup>R. L. Macklin and J. H. Gibbons, Phys. Rev. **159**, 1007 (1967).
- <sup>25</sup>H. Komano, PhD. thesis, Tokyo Institute of Technology, 1984.
- <sup>26</sup>H. N. Mülthei and B. Schorr, Nucl. Instrum. Methods **A257**, 371 (1987).
- <sup>27</sup>P. M. Endt and C. Van der Leun, Nucl. Phys. **A310**, 140 (1978).
- <sup>28</sup>J. G. Sullivan, G. G. Warner, R. C. Block, and R. W. Hockenbury, Rensselaer Polytechnic Institute Report RPI-328-155 (1969).
- <sup>29</sup>H. W. Schmitt *et al.*, Oak Ridge National Laboratory Report ORNL-2883 (1960).
- <sup>30</sup>ENDF/B-V data file for <sup>197</sup>Au (MAT=1379), evaluated by S. F. Mughabghab (1979).
- <sup>31</sup>H. Kitazawa, Triangle Universities Nuclear Laboratory Annual Report TUNL-XIX (1980), p. 114.
- <sup>32</sup>S. Raman, S. Kahane, and J. E. Lynn, in *Proceedings of the International Conference on Nuclear Data for Science and Technology, Mito, Japan, 1988*, edited by S. Igarasi (Saikon, Tokyo, 1988), p. 645.
- <sup>33</sup>C. Coceva, Y. K. Ho, M. Magnami, A. Mauri, and P. Bartolomei, in *Proceedings of the Sixth International Symposium on Capture Gamma-Ray Spectroscopy, Leuven, Belgium, 1987*, Inst. Phys. Conf. Series No. 88, edited by K. Abrahams and P. Van Assche (Institute of Physics, Bristol, U.K., 1988), p. 676.

- <sup>34</sup>R. J. Baglan, C. D. Bowman, and B. L. Berman, *Phys. Rev. C* **3**, 672 (1971).
- <sup>35</sup>R. C. Block, Z. M. Bartolome, J. R. Tatarczuck, W. R. Moyer, R. W. Hockenbury, and R. H. Wolfe, Rensselaer Polytechnic Institute Report RPI-328-142 (1968).
- <sup>36</sup>G. Nyström, B. Lundberg, and I. Bergqvist, *Phys. Scrip.* **4**, 95 (1971).
- <sup>37</sup>B. J. Allen, D. D. Cohen, and F. Z. Company, *J. Phys. G* **6**, 1173 (1980).
- <sup>38</sup>K. Hida, M. S. thesis, Tokyo Institute of Technology, 1980.
- <sup>39</sup>P. A. Moldauer, *Nucl. Phys.* **47**, 65 (1963).
- <sup>40</sup>R. F. Barrett and T. Terasawa, *Nucl. Phys.* **A240**, 445 (1975).
- <sup>41</sup>F. Meurders and G. de Korte, *Nucl. Phys.* **A249**, 205 (1975).
- <sup>42</sup>U. Sheib, A. Hofmann, G. Philipp, and F. Vogler, *Nucl. Phys.* **A203**, 177 (1973).
- <sup>43</sup>B. Čujec, *Phys. Rev.* **136**, B1305 (1964).
- <sup>44</sup>H. Schulz, H. J. Wiebicke, R. Fülle, D. Netzband, and K. Schlott, *Nucl. Phys.* **A159**, 324 (1970).
- <sup>45</sup>A. E. Litherland, H. McManus, E. B. Paul, D. A. Bromley, and H. E. Gove, *Can. J. Phys.* **36**, 378 (1958).
- <sup>46</sup>P. M. Endt, *At. Data Nucl. Data Tables* **19**, 49 (1977).
- <sup>47</sup>G. M. Crawley, C. Djalali, N. Marty, M. Morlet, A. Willis, N. Anantaraman, B. A. Brown, and A. Galonsky, *Phys. Rev. C* **39**, 311 (1989).
- <sup>48</sup>T. Tamura, *Rev. Mod. Phys.* **37**, 679 (1965); Oak Ridge National Laboratory Report ORNL-4152 (1967).